Weather and Climate Extremes 39 (2023) 100536

Contents lists available at ScienceDirect

Weather and Climate Extremes

journal homepage: www.elsevier.com/locate/wace

Where does the link between atmospheric moisture transport and extreme precipitation matter?

Luis Gimeno-Sotelo, Luis Gimeno *

Centro de Investigación Mariña, Universidade de Vigo, Environmental Physics Laboratory (EPhysLab), Ourense, Spain

ARTICLE INFO

Keywords:
Extreme precipitation
Moisture transport
Extreme value analysis

ABSTRACT

Atmospheric moisture transport is the primary component of the atmospheric branch of the water cycle, and its anomalies strongly influence drought and precipitation extremes. We utilised the full geographical and temporal spectrum of the ERA-5 reanalysis data and extreme value theory to identify regions where the atmospheric moisture transport, quantified as local integrated moisture vertical transport (IVT), influences daily extreme precipitation, and where this influence has a relevant dynamic component, which may alter the dependency between IVT and extreme precipitation as temperatures increase with climate change. We showed that this dependency is weak or negligible in tropical regions and strong but nonuniform in extratropical regions. Its influence is much greater in areas where the main moisture transport mechanisms occur, namely, atmospheric rivers, low-level jets, and tropical cyclones. The dynamic component of IVT, linked to wind, is highly consequential in regions with landfalling atmospheric rivers, landfalling tropical cyclones, or moisture-transporting low-level jets.

1. Introduction

Few topics bring as much consensus in the scientific community as the importance of the mechanisms of extreme precipitation and how they are influenced by climate change (Douville et al., 2021; Seneviratne et al., 2021; Caretta and Pörtner, 2022). In fact, extreme precipitation, in addition to being the main cause of floods and their dramatic socio-economic impacts, also arouses an important theoretical interest in relation to the mechanisms causing its intensification in response to a warming climate. Despite limitations in defining extreme precipitation periods and its various behaviours in tropical or extratropical regions (Zhang et al., 2019), a robust signal indicates that extreme precipitation increases globally with temperature, following the thermodynamic constraints imposed by the water-holding capacity of the atmosphere but varying regionally owing to atmospheric dynamical changes (O'Gorman, 2015; Bao et al., 2017).

Depending on the selected temporal and spatial domains, extreme precipitation can be caused by multiple meteorological systems. On the synoptic scale, tropical cyclones and monsoon lows in the tropics and baroclinic systems such as extratropical cyclones, warm conveyor belts, and fronts in the extratropics are the most prominent. The only common factors between these systems are the production of atmospheric instability with strong vertical motion and the potential for intense moisture transport to a region of extreme precipitation (De Vries, 2021). It is very difficult to generate intense precipitation with the sole humidity contained in the atmospheric column; strong and sustained moisture contributions are required from outside regions (Trenberth et al., 2003), in some cases very remote (Insua-Costa et al., 2022). Hence, great importance has been given to the main global mechanisms of moisture transport, namely the atmospheric rivers in the extratropics and the low-level jets (LLJs) in tropical regions (Gimeno et al., 2016).

Among the various methods of quantifying moisture transport (see Gimeno et al., 2012 for a review) the Eulerian scheme based on the integrated moisture vertical transport (IVT) has been the most widespread in extreme precipitation analyses, mainly due to its use in the identification and characterization of the atmospheric rivers (ARs) (Zhu and Newell, 1998; Gimeno et al., 2014; Payne et al., 2020). ARs are organised structures with high IVT that extend thousands of kilometres in length and a few hundred kilometres in width; they are responsible for approximately 90% of the meridional moisture transport from the subtropics to the extratropics (Zhu and Newell, 1998). Many global and regional studies have analysed the link between the current and future frequencies and intensities of ARs and precipitation extremes (e.g., at a global scale (Waliser and Guan, 2017), for the regional-scale current

* Corresponding author.
E-mail address: l.gimeno@uvigo.es (L. Gimeno).

https://doi.org/10.1016/j.wace.2022.100536
Received 22 May 2022; Received in revised form 1 December 2022; Accepted 3 December 2022
Available online 6 December 2022

climate (Lavers and Villarini, 2013; Ralph and Dettinger, 2012), and for the future climate (Gao et al., 2016; Whan et al., 2020). However, the relationship between IVT and extreme precipitation is not restricted only to the occurrence of ARs. There are values of IVT that are not categorised as ARs owing to the size of the structure (e.g., in the Mediterranean area including the Alpine region (Lorente-Plazas et al., 2020; Mahlstein et al., 2019)), the magnitude of the IVT, or the mechanism responsible for the high IVT values (e.g., tropical cyclones or LLJs-Gimeno et al., 2016-). Therefore, local IVT-extreme precipitation relationships have also been considered, so the IVT has been used as a precursor for extreme precipitation (Froidevaux and Martius, 2016) or to attribute singular extreme events to climate change (Reid et al., 2021). Notably, the IVT field is much more predictable than the precipitation field (Lavers et al., 2014, 2016), thereby increasing its already broad relevance.

Ultimately, the IVT is a product of humidity and wind; therefore, its values and sensitivity to climate change depend on those of humidity (thermodynamic component) and wind (dynamic component). This dichotomy translates into different influences from "windy ARs" versus "wet ARs". For example, in the west coast of the US, a main region for AR occurrence, more rainfall is associated with windy ARs than with wet ARs, but the latter is associated with higher AR frequency (Gonzales et al., 2020). In terms of sensitivity to climate change and, in particular, increases in global temperature, the thermodynamic component will follow the global dependence on humidity given by the Clausius–Clapeyron relationship, while the dynamic component will exhibit regional behaviours linked to changes in the atmospheric general circulation. For example, considering the end-of-century projections for a temperature increase of 3.5 °C, the thermodynamic component of the IVT increases uniformly worldwide at a rate of 20–40% per century, whereas the dynamic component decreases by 5–15% in the tropics and mid-latitudes and increases by a similar amount in polar regions (O'Brien et al., 2022).

However, the strength of the relationship between IVT and precipitation extremes varies greatly depending on the method chosen to define extreme precipitation and the IVT value and extension thresholds, as well as the region or season. There are regions where IVT has very little influence on precipitation extremes and others where its influence is decisive. Moreover, in the latter, the nexus may be more associated with either the thermodynamic or dynamic component of the IVT. Here, we utilised the full geographical and temporal spectrum of the state-of-the-art fifth-generation atmospheric reanalysis (ERA-5) data and the extreme value theory to model the relationships between daily extreme precipitation and IVT. This enabled us to determine where, when, and to what extent the relationship between IVT and extreme precipitation is important globally. Additionally, considering their importance in the context of climate change, we estimated the relative influence of the two IVT components, dynamic and thermodynamic, respectively represented by IVT/IWV and IWV, where IWV refers to the integrated water vapor along the atmospheric column, often referred to as precipitable water.

2. Data and methods

2.1. Data

We used data from the ERA-5 reanalysis (Hersbach, H. et al., 2020) -the most recent reanalysis from the European Centre for Medium-Range Weather Forecasts-to obtain daily values of precipitation, integrated moisture vertical transport (IVT) and integrated water vapor (IWV) for the period 1981–2020 at 0.5° resolution. IVT and IWV are defined as follows, in terms of the specific humidity, the eastward component of wind (u) and the northward component of wind (v):

$$IVT = \sqrt{\left(\frac{1}{g}\int_{\Omega} q\,u\,dp\right)^2 + \left(\frac{1}{g}\int_{\Omega} q\,v\,dp\right)^2} = \sqrt{IVT_u^2 + IVT_v^2} \quad \text{and}$$

$$IWV = \frac{1}{g}\int_{\Omega} q\,u\,dp \quad ,$$

where Ω refers to the entire atmospheric column and g to gravitational acceleration. The use of the entire atmospheric column is due to computational convenience, taking into account that the variables "total column water vapor" (IWV), "vertical integral of eastward water vapor flux" (IVT_u) and "vertical integral of northward water vapor flux" (IVT_v) from the ERA-5 reanalysis are so defined.

The main reason why the ERA-5 reanalysis was used in this study is because its primary aim was to identify the regions worldwide where the relationship between IVT and extreme precipitation is more intense on a global scale, and this reanalysis provides us with gridded data at a suitably high resolution for the meteorological interpretation of the worldwide and large-region results. To analyse how the link between the variables under study varies seasonally, the data were organised into four different sets according to the season: December–February (Northern Hemisphere Winter), March–May (Northern Hemisphere Spring), June–August (Northern Hemisphere Summer), and September–November (Northern Hemisphere Autumn).

2.2. Assessment of ERA-5 to evaluate daily and extreme precipitation and IWV

Reanalyses combine observations and circulation models to reconstruct past data with regular spatial and temporal resolution covering the entire globe, which is its main advantage and reason for its great use. Thus, they can generate data where there were no observations, the reason for their great success, but also the source of their strongest uncertainties. This forces us to be especially careful in its use and indicate where reanalyses are more appropriate and where less, especially in the use of daily and extreme data.

ERA-5 is the latest reanalysis generated by the European Centre for Medium-Range Weather Forecasts (Hersbach et al., 2020), and far exceeds its predecessor ERA-interim, and practically all reanalyses in use in quality for the study of the hydrological cycle (Nogueira, 2020). Due to its construction process, based on a circulation model, one of its strong points is the good reproduction of the large-scale general circulation of the atmosphere and it can be expected that it reproduces well its extremes, but it is more difficult to affirm that reproduces well daily and extreme values of precipitation and water column.

ERA-5 has been used since its launch in 2018 and there are not many previous assessment studies of daily precipitation and water column values at a global level, although there are some regional ones, especially linked to some type of precipitation -e.g. Hénin et al. (2018) in the Iberian Peninsula, Amjad et al. (2020) in Turkey, Bandhauer et al. (2022) in several European regions, Timmermans et al. (2019) or Xu et al. (2019) in the USA, Gleixner et al. (2020) in East Africa or Jiang et al. (2020) in Chinese mainland-. However, there are two global studies (Rivoire et al., 2021 for precipitation and Eiras Barca et al., 2022 for water column) that assess ERA-5 daily data against satellite data and one (Lavers et al., 2022) that assesses ERA5 daily precipitation data against gauge-based precipitation observations. They can help us to indicate where ERA-5 has more problems in reproducing daily and extreme precipitation and water column data and therefore the results of our study should be taken with caution.

Rivoire et al., 2021 assessed daily precipitation in ERA-5 against CMORPH satellite data (Joyce et al., 2004) over the entire globe for the period January 1979 to December 2018 in a regular grid with 0.25° resolution. To do this, they analysed the co-occurrence of precipitation extremes quantified by the hit rate, adjusting the extreme distributions using a generalized Pareto distribution for each grid point and

calculating the Kullback–Leibler divergence to quantify the distance between the entire EGPDs obtained from ERA-5 and the observations. In this study, it was concluded that ERA-5 and CMORPH precipitation intensity agree well over the midlatitudes and disagree over the tropics in all seasons. A view of the hit rate for events greater than the 95th percentile between ERA-5 and CMORPH (figure C2 in Rivoire et al., 2021) shows values that are higher than 70% in practically all the regions of interest in our study.

Lavers et al. (2022) used daily precipitation observations from 5 637 stations from 2001 to 2020 to assess daily precipitation in ERA-5, using the nearest neighbor approach to match the closest ERA-5 grid point to a station and the mean, the standard deviation of the differences and the Stable Equitable Error in Probability Space (SEEPS) score (Rodwell et al., 2010; Haiden et al., 2012) to estimate errors. They showed that the smallest ERA-5 errors occurred during winter in the extratropics and the largest in the tropics mostly across the Maritime Continent. An analysis of four extreme precipitation events showed a general agreement between the precipitation patterns from ERA-5 and the observations, although there are some limitations associated with strong convection and orography. The authors concluded that for both daily data and extreme precipitation events, ERA-5 is more skillful in the extratropics than in the tropics, and in extratropics during winter than during summer because of the convective systems.

Eiras-Barca et al. (2022) assessed daily ERA-5 integrated vertical water vapor column (IWV) data against the new Total Column Vater Vapor Data Record (CDR-2 (v2)) —developed by the European Space Agency (ESA) in coordination with the Satellite Application Facility on Climate Monitoring (CM SAF), for a unified grid of $0.5^\circ \times 0.5^\circ$ and the period July 2002–December 2017. The study was done globally but with a focus on regions of critical interest for moisture transport mechanisms (almost 40 000 atmospheric river (AR) and nocturnal low-level jet (NLLJ) events were identified on a global scale between 2002 and 2017). Results show low bias between ERA-5 versus CDR-2 in the regions of interest of our study (generally less than ± 2 kg m-2) and temporal correlations in the IWV fields above 0.8 in most areas. The highest disagreement was reported in the main tropical rainforest regions, which in general are not areas of critical interest for moisture transport phenomena.

Recently, an extension to the 50s has been made for the ERA-5 reanalysis (Bell et al., 2021), which would allow the period of record to be extended. This would substantially reduce the impact of sampling variability on the fitted extreme value distributions by increasing the annual maxima sample size. However, the extension of the ERA-5 reanalysis to 1950 is a new product and is still in the testing phase due to the large uncertainties it has in the upper air. Because the massive assimilation of satellite data occurs in the operational phase, since 1979, the vast majority of assimilable data at different vertical levels are those derived from radiosondes with limited spatial coverage. IVT is an extraordinarily sensitive variable to this since it integrates zonal and meridional winds and specific humidity data at multiple vertical levels, so a quality product cannot be expected. The extension to the 50s indeed incorporates some satellite data before the operational era, but in any case, they are very limited and do not guarantee adequate minimum spatial and temporal coverage. Therefore, introducing data before 1979 into our analysis would disturb the results, making them more uncertain, that is why we have limited the analysis to the most reliable period since 1980.

2.3. Statistical methods

We relied on the annual maxima method from the Extreme Value Theory (EVT). For extensive information about this method, see e.g. Coles (2001) and Beirlant et al. (2004). In short, for a given variable, the method consists of fitting a GEV distribution to the sample of the maximum annual values of that variable. Let Y be the random variable corresponding to the annual maxima of the variable under study; according to the annual maxima method, the distribution function of Y is assumed to have the following expression (GEV distribution function):

$$G(y;\ \mu,\sigma,\gamma) = \exp\left\{ -\left[1+\gamma\frac{y-\mu}{\sigma}\right]^{-1/\gamma}\right\} \text{with } 1+\gamma\frac{y-\mu}{\sigma}>0$$

where y is a value of the random variable Y, and $\mu \in \mathbb{R}, \sigma > 0,$ and $\gamma \in \mathbb{R}$ are the location, scale, and shape parameter of that distribution, respectively. The parameter μ quantifies the central tendency of the distribution, σ refers to its dispersion, and γ indicates whether the distribution is bounded and, if not, how "thick" the tail of the distribution is. If $\gamma < 0$, the distribution is bounded. If $\gamma > 0,$ it is unbounded and has a "heavy" tail; if $\gamma \to 0$, it is also unbounded and has an exponential tail. In the latter case, the GEV reduces to the Gumbel distribution, which takes the form:

$$G(y;\ \mu,\sigma) = \exp\left\{ -\exp\left[-\frac{y-\mu}{\sigma}\right]\right\}.$$

It is possible to express μ and σ in terms of a covariate z (non-stationary approach), for example, as linear functions: $\mu(z) = \beta_0 + \beta_1 z$ and $\sigma(z) = \theta_0 + \theta_1 z$.

For each season between 1981 and 2020, linearly detrended precipitation, IVT, IVT/IWV and IWV data were used to fit non-stationary GEV models to the annual maxima of precipitation at each grid point, considering separately the covariates IVT, IVT/IWV, and IWV (these covariates were centred and scaled before being used for the model fitting). The use of linearly detrended data is justified by the fact that the aim of this study is to assess the influence that these covariates have on extreme precipitation, regardless of the trends that the variables may have. Although the analysis is performed by means of linearly detrended data, it has been checked that the effect of removing trends is negligible in this study, as the use of detrended or non-detrended data produces very similar results in this case. The location and scale parameters were expressed as linear functions of the respective covariate, and the resulting coefficients $\beta_0, \beta_1, \theta_0$ and θ_1 , as well as the shape parameter γ , were estimated using maximum likelihood fitting using the software *R* (R Core Team, 2022; namely the *ismev* package -Heffernan and Stephenson, 2018). This estimation method enables the construction of asymptotic confidence intervals based on the normal approximation; see Casella and Berger (2002) for a theoretical explanation of maximum likelihood estimators and their asymptotic properties. Using confidence intervals, the significance of the coefficients β_0, β_1, θ_0 and θ_1 can be assessed; for a given confidence level, if the value 0 is contained in the confidence interval of a coefficient, that coefficient is judged not to be statistically significant at that level.

Regarding the assessment of the goodness of fit of the non-stationary GEV models, as pointed out in Coles (2001), there is not homogeneity in the distributional assumptions for each observation, that is, for each value of the covariate the parameters of the extreme value model take different values. Therefore, goodness-of-fit tests, which are common in the stationary case, are not simple to apply in the non-stationary one. Thus, following indications from Coles (2001), for $Y_z \sim GEV(\mu(z),\sigma(z),\gamma)$, we defined the standardized variables $\widetilde{Y}_z = \frac{1}{\gamma}\log\left\{1+\widehat{\gamma}\left(\frac{Y_z-\widehat{\mu}(z)}{\widehat{\sigma}(z)}\right)\right\}$, which are standard-Gumbel distributed, and produced probability and quantile plots of the observed $\widetilde{y}_z$ with respect to that distribution. The probability plot is constructed as follows: $\left\{\frac{i}{m+1}, \exp(-\exp(-\widetilde{y}_{(i)}));\ i=1,\ldots,m\right\}$

and the quantile plot:

$$\left\{\widetilde{y}_{(i)},\ -\log\left(-\log\left(\frac{i}{m+1}\right)\right);\ i=1,\ldots,m\right\}$$

where $\widetilde{y}_{(1)},\ldots,\widetilde{y}_{(m)}$ are the ordered values of the $\widetilde{y}_z$.

Having constructed these diagnostic plots, the goodness of fit of the non-stationary GEV models is assessed by means of the linearity of the points in those plots. As such, to have a metric that allows the assessment of global gridded data, we computed the R^2 of the linear regression

model which is associated to each plot, for all the non-stationary GEV models that were fitted.

Having fitted a GEV model to the annual maxima of precipitation, it is possible to estimate a *m*-year return level, which is the value of maximum precipitation which is exceeded on average once every *m* years. In a non-stationary framework with a covariate *z*, letting z^* be a fixed value for that covariate, the estimated *m*-year return level ($\widehat{y_m}$) can be calculated from the quantile function of the GEV distribution (denoted as $G^{\leftarrow}$) as follows:

$$\widehat{y_m} = G^{\leftarrow}\left(1 - \frac{1}{m}\ ;\ \widehat{\mu}(z^*), \widehat{\sigma}(z^*), \widehat{\gamma}\right)$$

where $\widehat{\mu}(z)$, $\widehat{\sigma}(z)$, and $\widehat{\gamma}$ refer to the estimated parameters of a non-stationary GEV model with location and scale parameters as a function of z (note that it is a conditional extreme value model). In this framework, the return levels estimates are conditional on specific realizations of the covariate, that is, a *m*-year return level is interpreted as a value that is exceeded once every 20 years when the covariate equals z^*.

In this study, we computed the percentage of variation in the estimated 20-year return level of maximum precipitation between a low and a high value of a given driver of that variable; thus, the 10th percentile and the 90th percentile of the centred and scaled covariates IVT, IVT/IWV, and IWV were calculated. High percentages in a region indicate that the corresponding covariate has a high influence on the precipitation maxima in that region. The computation of the estimated return levels was performed using the *R* package *evd* (Stephenson, 2002).

3. Results

3.1. Maximum precipitation and IVT: a first approach

A simple and intuitive way to visualise the fact that extreme precipitation is not related to extreme IVT everywhere in the same way is to show the patterns of the highest daily precipitation for the full analysed period, P_h, and the averaged IVT for the corresponding day, IVTp (Fig. 1; see Supplementary Fig. 1 for intermediate seasons).

A fundamental difference can be observed between the two patterns. In general, the P_h pattern is visually comparable with those of the mean precipitation or extreme precipitation above high percentiles (Supplementary Fig. 2 top), with the principal maxima in the Intertropical Convergence Zone (ITCZ) moving seasonally and secondary maxima in regions of occurrence of extratropical cyclones in both hemispheres with regional distinctions linked to tropical cyclones and monsoon circulations.

The IVTp pattern is no longer as similar to that of the mean or extreme IVT at high percentiles (Supplementary Fig. 2 bottom). Within the general pattern, there are coincidences in the extratropical regions of high IVT ("IVT storm tracks"), which migrate towards the poles in the summer of each hemisphere, and in the regions of very high IVT values that occur in June–August in the Indian monsoon region and the east coast of Asia; however, equatorial IVT maxima are not observed in the IVTp field, neither in the equatorial band of the Pacific easterly trade winds nor in the north-eastern South American continent. In large parts of the coincident regions, the IVTp value is notably above that of the 95th percentile, which indicates that very extreme IVT values correspond to the day of absolute maximum precipitation; therefore, a strong relationship exists between extreme precipitation and IVT in these

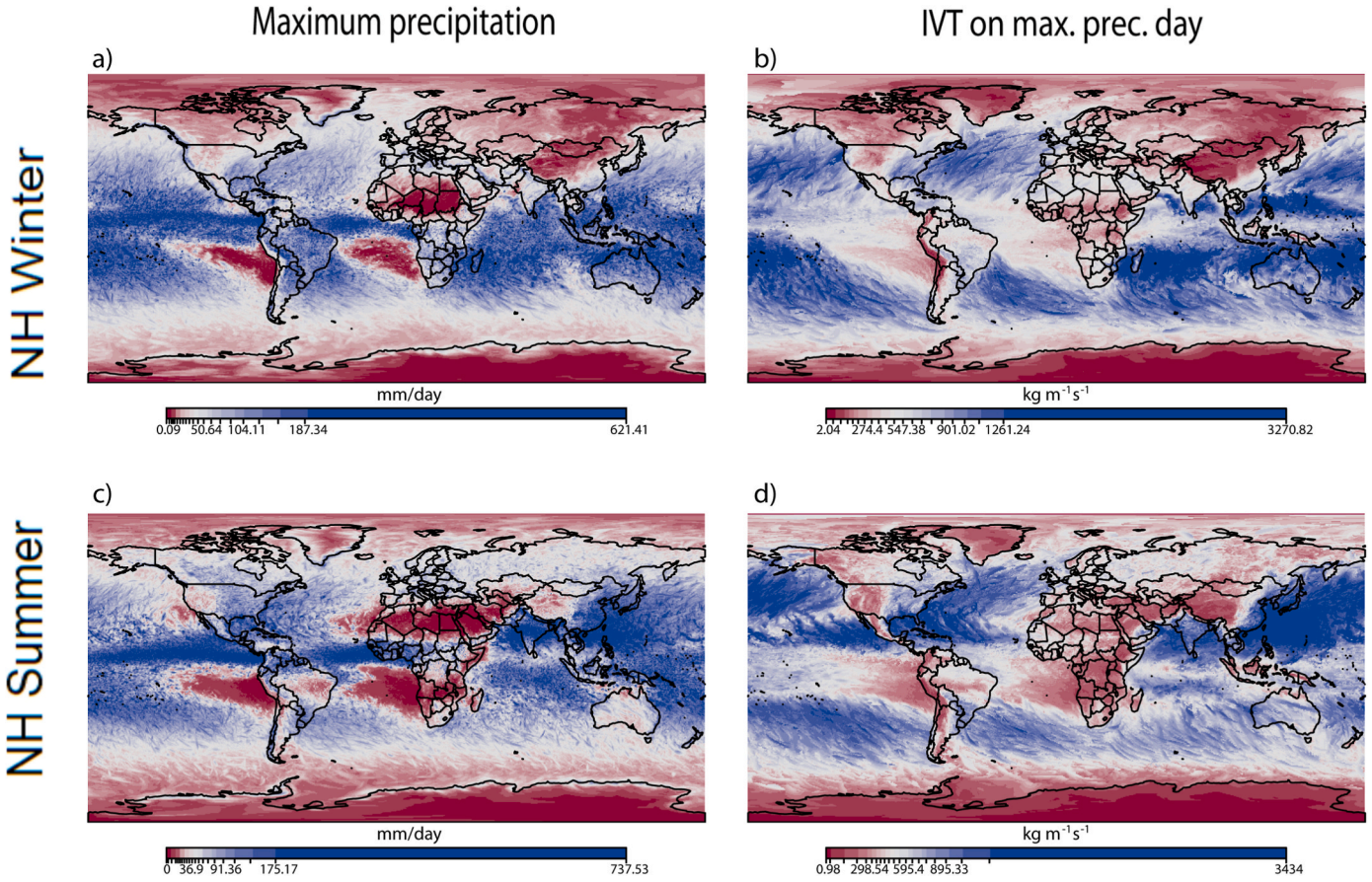

Fig. 1. Highest daily precipitation value and corresponding daily-averaged IVT value for a) and b) Northern Hemisphere Winter (December–February) and c) and d) Northern Hemisphere Summer (June–August), for the period 1981–2020.

regions.

Additionally, a careful visual analysis reveals the filamentous structures of the IVTp maxima, indicating that, in many cases, these values occurred on the same day through the same moisture transport structure. For example, this is very visible during both December–February and June–August in storm track regions owing to ARs (see Fig. 7 in Guan and Waliser, 2015) or during June–August in the North Atlantic owing to tropical cyclones (see Fig. 1 in Bloemendaal et al., 2020). The high coincidence in the IVTp maxima with P_h in the subtropical bands of maximum LLJs occurrence (see Fig. 4 in Algarra et al., 2019) is also noticeable. Therefore, the comparison between the P_h and IVTp patterns indicates that the relationship between extreme precipitation and IVT seems to be highly dependent upon the occurrence of the main global moisture transport mechanisms, namely ARs, LLJs, and tropical cyclones (Gimeno et al., 2016).

3.2. Regions and seasons in which IVT influences precipitation maxima

As described in Subsection 2.3, for each season, a non-stationary generalized extreme value (GEV) model was fitted to the annual precipitation maxima, allowing the location and scale parameters of the GEV distribution to vary linearly with IVT, IVT/IWV, and IWV. The goodness of fit of those models was assessed by means of the R^2 values for the linear models associated with the probability and quantile plots that were constructed as explained in Subsection 2.3; see Supplementary Figures 3,4 and 5. As can be seen from those figures, the R^2 values are very high (very close to 1) almost everywhere (and in every region of interest) for every season. Thus, these results indicate that the non-stationary GEV models that were fitted are adequate.

The location parameter (μ) of the GEV distribution measures the magnitude of the extreme precipitation and, considering that μ is expressed as a linear function of each covariate z, the slope (β_1) provides us with valuable information about the influence that this covariate has on the precipitation maxima. Fig. 2 (for intermediate seasons, see Supplementary Fig. 6) shows the maximum likelihood estimates for β_1 for the fitted GEV models, considering IVT and IVT/IWV separately as a covariate. For notation simplicity, those estimates are denoted by $\widehat{\beta}_{IVT}$ and $\widehat{\beta}_{IVT/IWV}$. Only significant values of $\widehat{\beta}_{IVT}$ and $\widehat{\beta}_{IVT/IWV}$ were plotted, and their significance was assessed in terms of their normal approximation confidence intervals (see Subsection 2.3). From this figure, we quantified the influence that IVT and its dynamic component, IVT/IWV, had on precipitation maxima.

The $\widehat{\beta}_{IVT}$ pattern (Fig. 2a,c) shows overlapping occurrences of the main moisture transport mechanisms (Fig. 3). Thus, in general, this relationship was strong in the subtropical regions of both hemispheres, practically null in the tropical regions, and moderate in the extratropical regions; in the latter case, it oscillated between an almost negligible relationship in the Southern Hemisphere (due to the minimal presence of continental regions) to a stronger one in the Northern Hemisphere. Additionally, the influence of ARs was observed in a continuous subtropical band of strong influence along the coastal regions of the continents and extending to high latitudes, including the polar ones, with greater intensity during their respective winters. Tropical cyclones influenced a strong relationship between IVT and extreme precipitation in all areas of TC occurrence in their corresponding summers. The influence of LLJs was apparent in the monsoon regions of the Asian

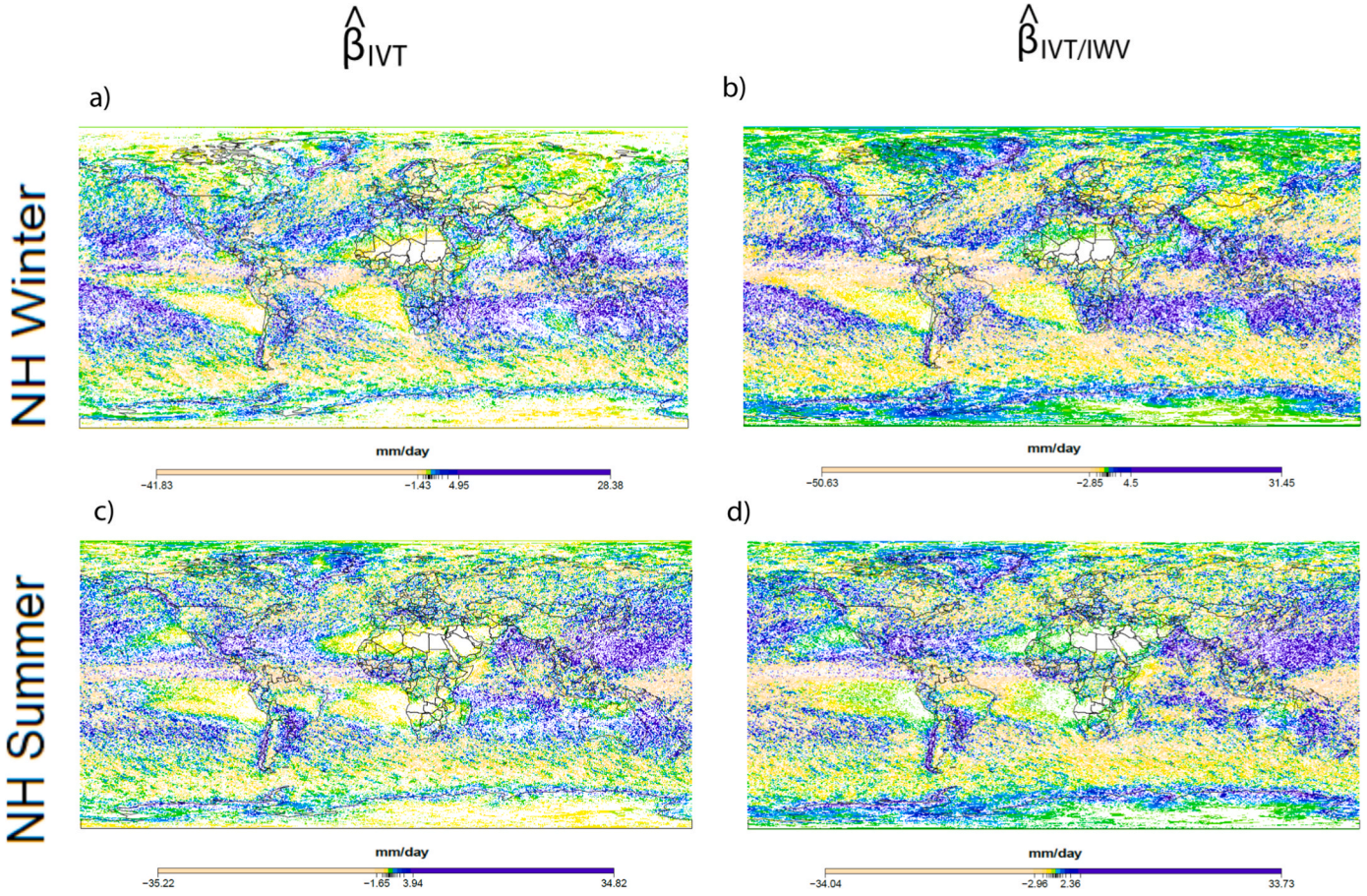

Fig. 2. Spatial patterns of the significant values of the estimated coefficient that represents the influence of IVT (a) and c)) and IVT/IWV (b) and d)) on maximum precipitation according to the GEV analysis (95% confidence level), for Northern Hemisphere Winter (December–February) and Northern Hemisphere Summer (June–August), respectively, for the period 1981–2020.

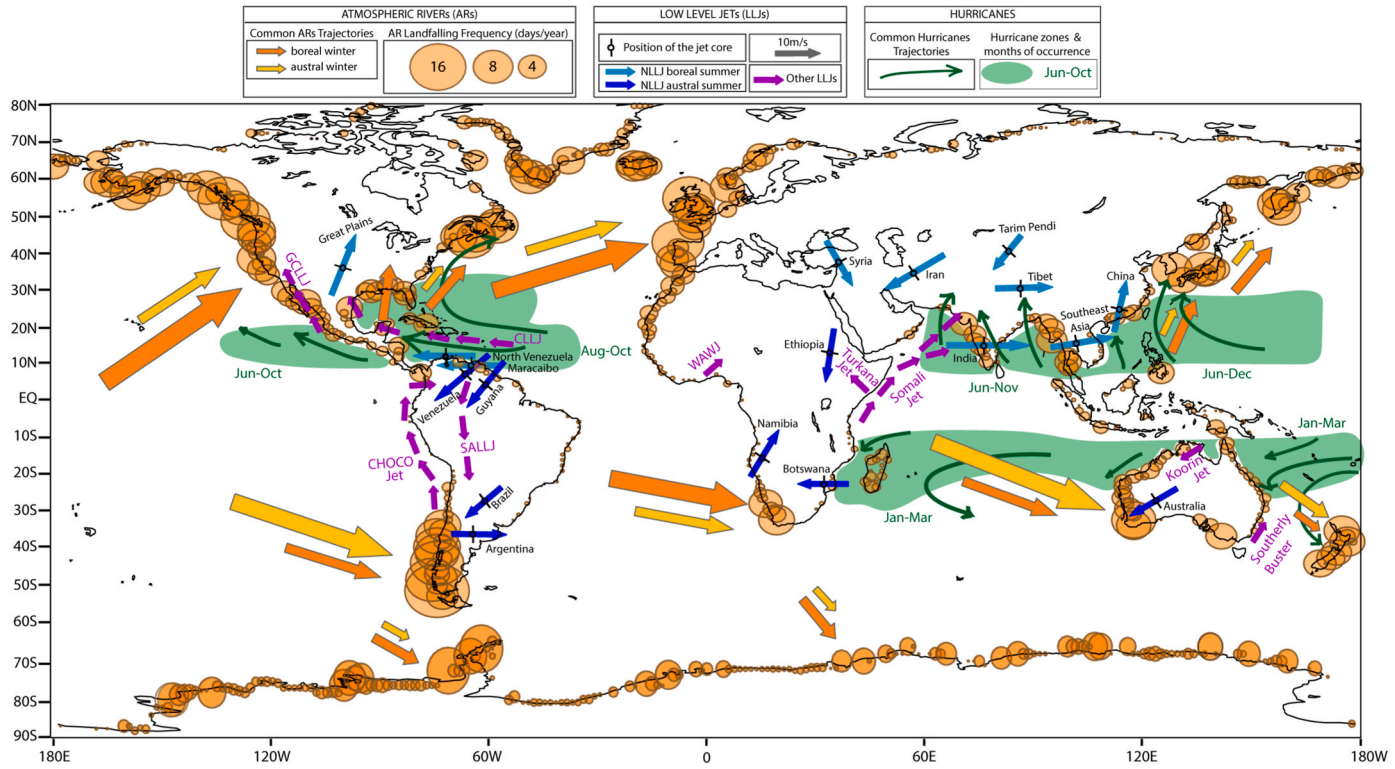

Fig. 3. Main regions where atmospheric rivers (ARs), low-level jets (LLJs), and tropical cyclones (TCs) occur. This figure was adapted from Gimeno et al. (2016). Orange arrows indicate the direction of ARs and orange circles show the frequency of landfalling ARs (days/year), based on Guan and Waliser (2015). Locations of nocturnal LLJs, as described by Rife et al. (2010), are shown as blue arrows, and their names are also displayed. The size of the arrow is scaled to the speed in the core of the jet. Green areas and dates indicate the regions and periods of tropical cyclone occurrence (Source: International Best Track Archive for Climate Stewardship, NOAA (Knapp et al., 2010)). (For interpretation of the references to colour in this figure legend, the reader is referred to the Web version of this article.)

continent during June–August, and in the south-eastern region of the South American continent.

This pattern is much more notable when the influence of the dynamic component of the IVT, calculated as $\widehat{\beta}_{IVT/IWV}$, is examined (Fig. 2b,d). At a continental level, this dynamic component influences extreme precipitation in the main regions where ARs make landfall (Fig. 3), such as the western North American, European, or South American coasts during their respective winters; in regions where TCs make landfall during summers, such as the North American and south-eastern Asian coasts; and in regions where LLJs cross continents, such as those associated with the Indian monsoon or the easternmost branch of the South American low-level jet.

In the remaining regions where IVT influences extreme precipitation, this influence is exclusively due to the thermodynamic component of the IVT, associated with the IWV (Supplementary Fig. 7). This supplementary figure represents the significant values of $\widehat{\beta}_{IWV}$, that is, the estimate of the slope (β_1) considering IWV as the covariate.

3.3. Contribution of the dynamic component of IVT to the precipitation maxima

The dynamic component of IVT, estimated as the ratio IVT/IWV, represents the vertically averaged wind, weighted by the specific humidity at each height. Its variations are related to changes in the magnitude of moisture-transporting winds; hence, they are linked to changes in atmospheric circulation.

Fig. 4 shows a finer regional analysis than Fig. 2, by representing the percentage change in the estimated 20-year return levels of the maximum precipitation when the covariate IVT/IWV is low and high (the 10th and 90th percentiles). This represents the change in the maximum precipitation value that is expected to occur on average once every 20 years, for a high versus a low dynamic component of IVT (it is important to remind that the return levels estimates are conditional on specific realizations of the covariate).

As can be seen in Fig. 4, there are regions in which changes were approximately 50% or higher. These occurred during the boreal winter on the west coast of North America, west coast of the Mediterranean, east coast of southern Africa, and central and western Australia. During the boreal summer, areas of relevant change were observed along the coasts of the Gulf of Mexico, the Caribbean, and Australia, the central regions of South America, and the north-western Indian subcontinent. It is in these regions that the greatest modifications of the relationship between IVT and extreme precipitation can be expected in a changing climate. These changes have already been observed in the present warming climate. A recent study observed changes in the estimated probability of concurrent IVT and precipitation extremes in most AR-landfall regions when comparing a recent (warmer) period versus a previous (colder) period (Gimeno-Sotelo and Gimeno, 2022).

4. Discussion and conclusion

We identified regions where atmospheric moisture transport, quantified as IVT, influences the daily extreme precipitation. Moreover, we determined where this influence has a relevant dynamic component, which may cause the relationship between IVT and extreme precipitation to change due to increased temperatures linked to climate change. Three important conclusions can be drawn from the study:

- The relationship between the IVT and extreme daily precipitation is very weak or even negligible in tropical regions. Because very high values of water vapor already exist in the tropics, a continuous and high external moisture contribution is not necessary to provide water vapor for extreme precipitation. In situations of atmospheric

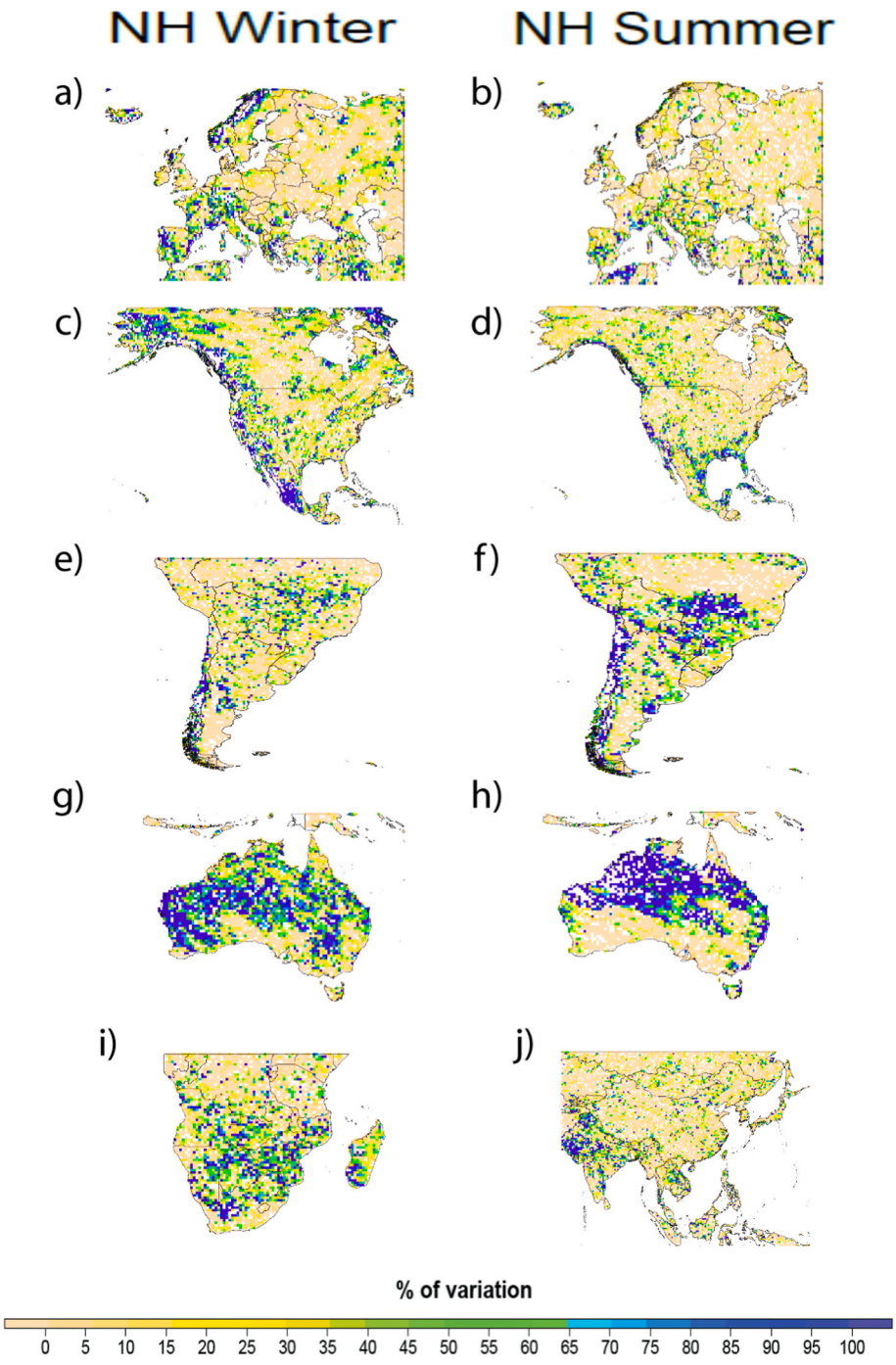

Fig. 4. Spatial pattern of the percentage of variation for the estimated 20-year return levels of maximum precipitation between the 10th and 90th percentiles of IVT/IWV, for the period 1981–2020. (a), (c), (e), and (g) refer to the results for Europe, North America, South America, and Australia during Northern Hemisphere Winter (December–February); b), d), f), and h) indicate the same regions during Northern Hemisphere Summer (June–August). i) corresponds to Southern Africa during NH Winter, and j) refers to the Asian monsoon region during NH Summer.

instability, the necessary water vapor to potentially generate extreme precipitation is already present. This agrees with the auxiliary results presented in this article concerning the dependence of IWV on extreme precipitation and the results reached in a recent paper, where a strong relationship between extremes of IWV and extreme daily precipitation was demonstrated (Kim et al., 2022).

- In extratropical regions, IVT strongly influences extreme precipitation, but not uniformly. Its influence is much greater in areas where the main modes of moisture transport occur, namely: (i) in the extensions of the subtropical band of moisture transport towards high latitudes in coastal regions, thereby revealing a signature of the ARs; (ii) in the regions and seasons of occurrence of tropical cyclones; and (iii) in the areas where strong low-level jet systems occur, which are frequently associated with monsoon circulations. In the polar regions of both hemispheres, the influence is restricted to the ARs.
- The dynamic component of IVT, linked to the wind, is highly important in the relationship between IVT and extreme precipitation in many regions of great meteorological and socioeconomic interest, such as: (i) the primary regions where ARs make landfall, including the west coasts of North America, South America, and Europe; (ii) the main regions of tropical cyclone landfalls, such as the southeast coast of North America, the Caribbean, and southeast Asia; and (iii) the regions influenced by large LLJs that transport moisture, such as the Indian monsoon region and southern South America. In these regions, the importance of the thermodynamic component of the IVT, associated with the IWV, decreases; Kim et al., 2022 also noted this, finding a smaller impact from the IWV on non-tropical extreme

precipitation events, except for continental areas of America and Eurasia that are far inland.

Our study has important practical implications deriving from the identification of regions and seasons during which studying the relationship between IVT and extreme precipitation is particularly important. This also implies that the study of the predictability of IVT in these specific regions and seasons can improve the predictability of daily precipitation extremes in those regions.

However, this study also has important theoretical implications. In the regions where the dynamic component of the IVT is important for extreme precipitation, the magnitude of the relationship between IVT and extreme precipitation may be more altered by climate change. As humidity, which defines the thermodynamic component of the IVT, will influence both IVT and extreme precipitation similarly, in those regions where the dynamic component of the IVT is important, we should expect greater changes in the dependence between IVT and extreme precipitation in the future.

This study has some limitations associated with the quality of the reanalysis precipitation data, which is generally low for regions with less dense instrument networks. Additionally, the coarse resolution of the data of the reanalysis necessitated further regional analysis in areas with complex orography or where small-scale convective processes are relevant. In particular, ERA-5 should be used carefully to study extreme precipitation over the tropics and IWV in the main tropical rainforest regions, but its confidence is high in the regions (extratropical) and seasons (winter) where the main results of our study are reached. Furthermore, the sample size may be seen as an important limitation (see Li et al., 2019) because, for each season, we used 40 annual precipitation maxima for model fitting; therefore, the parameter estimates may have been affected by sampling variability, as noted by Su and Smith (2021). If the period of reliable worldwide gridded data for IVT and precipitation were larger, the obtained results for the GEV analysis would be more robust. A comprehensive validation of the quality of the daily data of winds and specific humidity in the upper air of the recently released extension of ERA-5 to the 50s is clearly necessary for this purpose.

CRediT authorship contribution statement

Luis Gimeno-Sotelo: Formal analysis, Visualization, Writing – original draft, Writing – review & editing. **Luis Gimeno:** Conceptualization, Resources, Writing – original draft, Writing – review & editing, Supervision, Funding acquisition.

Declaration of competing interest

The authors declare that they have no known competing financial interests or personal relationships that could have appeared to influence the work reported in this paper.

Data availability

ERA-5 reanalysis data are publicly available and can be obtained from https://cds.climate.copernicus.eu.

Acknowledgements

This work is part of the SETESTRELO project (grant no. PID2021-122314OB-I00) funded by the Ministerio de Ciencia e Innovación, Spain. The EPhysLab group was co-funded by Xunta de Galicia, Consellería de Cultura, Educación e Universidade, under project ED431C 2021/44 “Programa de Consolidación e Estructuración de Unidades de Investigación Competitivas”. Luis Gimeno-Sotelo was supported by a UVigo PhD grant (“Axudas para contratos predoutorais da Universidade de Vigo”). The authors would like to especially thank Raquel Nieto for her assistance in the design of the figures, and Iago Algarra and Marta Vázquez for downloading necessary data for the study.

Appendix A. Supplementary data

Supplementary data to this article can be found online at https://doi.org/10.1016/j.wace.2022.100536.

References

Algarra, I., Eiras-Barca, J., Nieto, R., Gimeno, L., 2019. Global climatology of nocturnal low-level jets and associated moisture sources and sinks. Atmos. Res. 229, 39–59. https://doi.org/10.1016/j.atmosres.2019.06.016.

Amjad, M., Yilmaz, M.T., Yucel, I., Yilmaz, K.K., 2020. Performance evaluation of satellite- and model-based precipitation products over varying climate and complex topography. J. Hydrol. 584 (February), 124707 https://doi.org/10.1016/j.jhydrol.2020.124707.

Bandhauer, M., Isotta, F., Lakatos, M., Lussana, C., Båserud, L., Izsák, B., Szentes, O., Tveito, O.E., Frei, C., 2022. Evaluation of daily precipitation analyses in E-OBS (v19.0e) and ERA5 by comparison to regional high-resolution datasets in European regions. Int. J. Climatol. 42 (2), 727–747. https://doi.org/10.1002/joc.7269.

Bao, J., Sherwood, S.C., Alexander, L.V., Evans, J.P., 2017. Future increases in extreme precipitation exceed observed scaling rates. Nat. Clim. Change 7 (2), 128–132. https://doi.org/10.1038/nclimate3201.

Beirlant, J., Goegebeur, Y., Segers, J., Teugels, J.L., 2004. Statistics of Extremes: Theory and Applications. John Wiley & Sons, Chichester.

Bell, B., Hersbach, H., Simmons, A., Berrisford, P., Dahlgren, P., Horányi, A., et al., 2021. The ERA5 global reanalysis: preliminary extension to 1950. Q. J. R. Meteorol. Soc. 147 (741), 4186–4227. https://doi.org/10.1002/qj.4174. Available from:

Bloemendaal, N., et al., 2020. Generation of a global synthetic tropical cyclone hazard dataset using STORM. Sci. Data 7 (1), 1–12. https://doi.org/10.1038/s41597-020-0381-2.

Caretta, M.A., et al., 2022. Water. In: Climate Change 2022: Impacts, Adaptation, and Vulnerability. Contribution of Working Group II to the Sixth Assessment Report of the Intergovernmental Panel on Climate Change [Pörtner, H.O. , et al.]. Cambridge University Press (in press).

Casella, G., Berger, R.L., 2002. Statistical Inference, second ed. Duxbury Press, Pacific Grove.

Coles, S., 2001. An Introduction to Statistical Modeling of Extreme Values. Springer, London.

De Vries, A.J., 2021. A global climatological perspective on the importance of Rossby wave breaking and intense moisture transport for extreme precipitation events. Weather and Climate Dynamics 2 (1), 129–161. https://doi.org/10.5194/wcd-2-129-2021.

Douville, H., et al., 2021. Water cycle changes. In: Climate Change 2021: The Physical Science Basis. Contribution of Working Group I to the Sixth Assessment Report of the Intergovernmental Panel on Climate Change [Masson-Delmotte, V., et al.]. Cambridge University Press (in press).

Eiras-Barca, J., Algarra, I., Nieto, R., Schröder, M., Hegglin, M.I., Gimeno, L., 2022. Analysis of the main source regions of moisture transport events with the new ESA CCI/CM-SAF Total Column Water Vapour Climate Data Record (v2). Q. J. R. Meteorol. Soc. https://doi.org/10.1002/qj.4358.

Froidevaux, P., Martius, O., 2016. Exceptional integrated vapour transport toward orography: an important precursor to severe floods in Switzerland. Q. J. R. Meteorol. Soc. 142 (698), 1997. https://doi.org/10.1002/qj.2793, 201.

Gao, Y., Lu, J., Leung, L.R., 2016. Uncertainties in projecting future changes in atmospheric rivers and their impacts on heavy precipitation over Europe. J. Clim. 29 (18), 6711–6726, 2016. https://www.jstor.org/stable/26385654.

Gimeno, L., et al., 2012. Oceanic and terrestrial sources of continental precipitation. Rev. Geophys. 50, 4. https://doi.org/10.1029/2012RG000389.

Gimeno, L., Nieto, R., Vázquez, M., Lavers, D.A., 2014. Atmospheric rivers: a mini-review. Front. Earth Sci. 2, 2. https://doi.org/10.3389/feart.2014.00002.

Gimeno, L., et al., 2016. Major mechanisms of atmospheric moisture transport and their role in extreme precipitation events. Annu. Rev. Environ. Resour. 41, 117–141. https://doi.org/10.1146/annurev-environ-110615-085558.

Gimeno-Sotelo, L., Gimeno, L., 2022. Concurrent extreme events of atmospheric moisture transport and continental precipitation: the role of landfalling atmospheric rivers. Atmos. Res. 278, 106356 https://doi.org/10.1016/j.atmosres.2022.106356.

Gleixner, S., Demissie, T., Diro, G.T., 2020. Did ERA5 improve temperature and precipitation reanalysis over East Africa? Atmosphere 11 (9), 996–1019. https://doi.org/10.3390/atmos11090996.

Gonzales, K.R., Swain, D.L., Barnes, E.A., Diffenbaugh, N.S., 2020. Moisture-versus wind-dominated flavors of atmospheric rivers. Geophys. Res. Lett. 47, 23. https://doi.org/10.1029/2020GL090042.

Guan, B., Waliser, D.E., 2015. Detection of atmospheric rivers: evaluation and application of an algorithm for global studies. J. Geophys. Res. Atmos. 120 (24), 12514–12535. https://doi.org/10.1002/2015JD024257.

Haiden, T., Rodwell, M.J., Richardson, D.S., Okagaki, A., Robinson, T., Hewson, T.D., 2012. Intercomparison of global model precipitation forecast skill in 2010/11 using the SEEPS score. Mon. Weather Rev. 140, 2720–2733. https://doi.org/10.1175/MWR-D-11-00301.1.

Heffernan, J.E., Stephenson, A.G., 2018. Ismev: an introduction to statistical modeling of extreme values. R package version 1.42. https://CRAN.R-project.org/package=ismev.

Hénin, R., Liberato, M., Ramos, A., Gouveia, C., 2018. Assessing the use of satellite-based estimates and high-resolution precipitation datasets for the study of extreme precipitation events over the Iberian Peninsula. Water 10 (11), 1688. https://doi.org/10.3390/w10111688.

Hersbach, H., et al., 2020. The ERA5 global reanalysis. Q. J. R. Meteorol. Soc. 146 (730), 1999–2049. https://doi.org/10.1002/qj.3803.

Insua-Costa, D., Senande-Rivera, M., Llasat, M.C., Miguez-Macho, G., 2022. A global perspective on western Mediterranean precipitation extremes. npj Climate and Atmospheric Science 5 (1), 1–7. https://doi.org/10.1038/s41612-022-00234-w.

Jiang, Q., Li, W., Fan, Z., He, X., Sun, W., Chen, S., et al., 2020. Evaluation of the ERA5 reanalysis precipitation dataset over Chinese Mainland. J. Hydrol., 125660 https://doi.org/10.1016/j.jhydrol.2020.125660. October.

Joyce, R.J., Janowiak, J.E., Arkin, P.A., Xie, P., 2004. CMORPH: a method that produces global precipitation estimates from passive microwave and infrared data at high spatial and temporal resolution. J. Hydrometeorol. 5 (3), 487–503. https://doi.org/10.1175/1525-7541(2004)005⟨0487:CAMTPG⟩2.0.CO;2.

Kim, S., Sharma, A., Wasko, C., Nathan, R., 2022. Linking total precipitable water to precipitation extremes globally. Earth's Future 10, e2021EF002473. https://doi.org/10.1029/2021EF002473.

Knapp, K.R., et al., 2010. NCDC International Best Track Archive for Climate Stewardship (IBTrACS) Project, Version 3. NOAA National Centers for Environmental Information. https://doi.org/10.7289/V5NK3BZP.

Lavers, D.A., Villarini, G., 2013. The nexus between atmospheric rivers and extreme precipitation across Europe. Geophys. Res. Lett. 40 (12), 3259–3264. https://doi.org/10.1002/grl.50636.

Lavers, D.A., Pappenberger, F., Zsoter, E., 2014. Extending medium-range predictability of extreme hydrological events in Europe. Nat. Commun. 5 (1), 1–7. https://doi.org/10.1038/ncomms6382.

Lavers, D.A., Pappenberger, F., Richardson, D.S., Zsoter, E., 2016. ECMWF Extreme Forecast Index for water vapor transport: a forecast tool for atmospheric rivers and extreme precipitation. Geophys. Res. Lett. 43 (22), 11–852. https://doi.org/10.1002/2016GL07132.

Lavers, D.A., Simmons, A., Vamborg, F., M, J., 2022. An evaluation of ERA5 precipitation for climate monitoring. Q. J. R. Meteorol. Soc. 1–14. https://doi.org/10.1002/qj.4351. Available from:

Li, C., Zwiers, F., Zhang, X., Li, G., 2019. How much information is required to well constrain local estimates of future precipitation extremes? Earth's Future 7 (1), 11–24.

Lorente-Plazas, R., et al., 2020. Unusual atmospheric-river-like structures coming from Africa induce extreme precipitation over the western Mediterranean Sea. J. Geophys. Res. Atmos. 125, 2. https://doi.org/10.1029/2019JD031280.

Mahlstein, I., Bhend, J., Spirig, C., Martius, O., 2019. Developing an automated medium-range flood awareness system for Switzerland based on probabilistic forecasts of integrated water vapor fluxes. Weather Forecast. 34 (6), 1759–1776. https://doi.org/10.1175/WAF-D-18-0189.1.

Nogueira, M., 2020. Inter-comparison of ERA-5, ERA-interim and GPCP rainfall over the last 40 years: process-based analysis of systematic and random differences. J. Hydrol. 583 (August 2019), 124632 https://doi.org/10.1016/j.jhydrol.2020.124632.

O'Brien, T.A., et al., 2022. Increases in future AR count and size: overview of the ARTMIP Tier 2 CMIP5/6 experiment. J. Geophys. Res. Atmos. 127, 6. https://doi.org/10.1029/2021JD036013.

O'Gorman, P.A., 2015. Precipitation extremes under climate change. Curr. Clim. Change Rep. 1 (2), 49–59. https://doi.org/10.1007/s40641-015-0009-3.

Payne, A.E., et al., 2020. Responses and impacts of atmospheric rivers to climate change. Nat. Rev. Earth Environ. 1 (3), 143–157. https://doi.org/10.1038/s43017-020-0030-5.

R Core Team. R, 2022. A Language and Environment for Statistical Computing. R Foundation for Statistical Computing, Vienna, Austria. URL. https://www.R-project.org/.

Ralph, F.M., Dettinger, M.D., 2012. Historical and national perspectives on extreme West Coast precipitation associated with atmospheric rivers during December 2010. Bull. Am. Meteorol. Soc. 93 (6), 783–790. https://doi.org/10.1175/BAMS-D-11-00188.1.

Reid, K.J., O'Brien, T.A., King, A.D., Lane, T.P., 2021. Extreme water vapor transport during the March 2021 sydney floods in the context of climate projections. Geophys. Res. Lett. 48, 22. https://doi.org/10.1029/2021GL095335.

Rife, D.L., Pinto, J.O., Monaghan, A.J., Davis, C.A., Hannan, J.R., 2010. Global distribution and characteristics of diurnally varying low-level jets. J. Clim. 23 (19), 5041–5064. https://doi.org/10.1175/2010JCLI3514.1.

Rivoire, P., Martius, O., Naveau, P., 2021. A comparison of moderate and extreme ERA-5 daily precipitation with two observational data sets. Earth Space Sci. 8, e2020EA001633 https://doi.org/10.1029/2020EA001633.

Rodwell, M.J., Richardson, D.S., Hewson, T.D., Haiden, T., 2010. A new equitable score suitable for verifying precipitation in numerical weather prediction. Q. J. R. Meteorol. Soc. 136, 1344–1363. https://doi.org/10.1002/qj.656.

Seneviratne, S.I., et al., 2021. Weather and climate extreme events in a changing climate. In: Climate Change 2021: The Physical Science Basis. Contribution of Working Group I to the Sixth Assessment Report of the Intergovernmental Panel on Climate Change [Masson-Delmotte, V., et al.]. Cambridge University Press (Press).

Stephenson, A.G., 2002. Evd: extreme value distributions. R. News 2 (2), 31–32. URL: https://CRAN.R-project.org/doc/Rnews/.

Su, Y., Smith, J.A., 2021. An atmospheric water balance perspective on extreme rainfall potential for the contiguous US. Water Resour. Res. 57, 4. https://doi.org/10.1029/2020WR028387.

Timmermans, B., Wehner, M., Cooley, D., O'Brien, T., Krishnan, H., 2019. An evaluation of the consistency of extremes in gridded precipitation data sets. Clim. Dynam. 52 (11), 6651–6670. https://doi.org/10.1007/s00382-018-4537-0.

Trenberth, K.E., Dai, A., Rasmussen, R.M., Parsons, D.B., 2003. The changing character of precipitation. Bull. Am. Meteorol. Soc. 84 (9), 1205–1218. https://doi.org/10.1175/BAMS-84-9-1205.

Waliser, D., Guan, B., 2017. Extreme winds and precipitation during landfall of atmospheric rivers. Nat. Geosci. 10 (3), 179–183. https://doi.org/10.1038/ngeo2894.

Whan, K., Sillmann, J., Schaller, N., Haarsma, R., 2020. Future changes in atmospheric rivers and extreme precipitation in Norway. Clim. Dynam. 54 (3), 2071–2084. https://doi.org/10.1007/s00382-019-05099-z.

Xu, X., Frey, S.K., Boluwade, A., Erler, A.R., Khader, O., Lapen, D.R., Sudicky, E., 2019. Evaluation of variability among different precipitation products in the Northern Great Plains. J. Hydrol.: Reg. Stud. 24 (May), 100608 https://doi.org/10.1016/j.ejrh.2019.100608.

Zhang, W., Villarini, G., Wehner, M., 2019. Contrasting the responses of extreme precipitation to changes in surface air and dew point temperatures. Climatic Change 154 (1), 257–271. https://doi.org/10.1007/s10584-019-02415-8.

Zhu, Y., Newell, R.E., 1998. A proposed algorithm for moisture fluxes from atmospheric rivers. Mon. Weather Rev. 126 (3), 725–735.